# CHAPTER FOUR

# *K*-ω MODELLING METHOD FOR AN INFINITE SOLID

## 4.1 Introduction

### *4.1.1 Purpose of this chapter*

In this chapter a more sophisticated modelling technique (the *k*-ω method) is presented. The method assumes the conduit is a vertically oriented, partially viscous fluid filled cylinder embedded in an infinite solid. Perturbations in matched boundary conditions at the conduit wall allow moving and extended sources to be modelled in addition to point sources. This is an important breakthrough in volcano seismology. Even if these other sources are found not to be applicable to volcano-seismic signals, at least they can now by rejected on a quantitative basis, rather than through laziness or ignorance.

The method was derived from first principles, but follows an outline given by *Theisse* [1996], However, the treatment here is much more thorough and rigorous, and uses a much improved nomenclature. The method has also been extended to include several new source types [Section 4.4], including advective overpressure which is described by a line source, and a rising magma source with a pressure gradient; these are derived in full. Some of the mathematics for this method cannot be found in previously published work and is included in Appendices.

The method is thoroughly tested in Section 4.5, which is entirely original work, prior to its application to Stromboli in Chapter 5.

### 4.1.2 Review of modelling techniques

Broadband recordings such as those at Stromboli [*Neuberg et al*., 1994] and Aso volcano [*Kaneshima et al*., 1996] have revealed long-period phases that are believed to be a direct response to the magma movement or pressurization of the volcanic edifice. In order to understand these signals, modelling is required.

A dilatational point source [*Anderson*, 1936; *Mogi*, 1958] can be used to estimate the depth and volume change of a spherical magma chamber, and a simple formula can be used to estimate the pressure change required to cause such a volume change. This 'Mogi' source is static and can be used very effectively to model the deformation of the free surface in response to a change in source volume at a given depth, but it cannot be used directly to calculate seismograms. Neither can it be used directly to model moving sources or extended sources. The decay law method presented in Chapter 3 is similar to the Mogi model, but more useful for seismology because both near and far field terms are considered, and because line sources can also be modelled.

The opposite extreme is to use finite element modelling [*Stephen et al*., 1985; *Randall et al.,* 1991; *Ohminato and Chouet*, 1997]. With such a technique the physical parameters of each model element are initialised, and then the model is evolved, each element following a set of simplified physical laws. Such a method is computationally expensive, and difficult to modify, but given sufficient time and perseverance, models of any complexity can be computed to any level of precision.

Boundary element methods have been implemented by several authors to calculate synthetic borehole seismograms in a half-space and in a horizontally stratified medium [e.g. *Bouchon,* 1993; *Dong et al.*, 1995]. The technique is based on Huygens' principle: several points along the cylindrical borehole boundary act as secondary sources for a primary source in the fluid. The parallels between a fluid-filled cylindrical borehole and a vertically oriented volcanic conduit are obvious.

The method described in this chapter is also derived from borehole seismology. Assuming a cylindrical fluid-filled borehole, *Biot* [1952] solved the wave equation in the wavenumber-frequency domain[1], assuming continuity of radial stress and displacement at the borehole wall, in order to study interface waves (Stoneley waves) propagating in the vicinity of the borehole wall. *Cheng and Toksoz* [1980] took this method a little further and investigated another wave type ('pseudo-

[1] This is done because it makes the mathematics easier; see equation A-18.

Rayleigh' waves), and calculated synthetic micro-seismograms. *Theisse* [1996] adapted this method for modelling the deformation at volcanoes by introducing pressure and shear stress fluctuations at the conduit wall, which can be employed to simulate any type of source. This method is further developed here and new types of moving and extended sources are introduced, as these may be relevant for very long period seismic signals and deformation signals, such as those observed at Stromboli and Aso. Because the method is based on a set of analytic calculations, computation is relatively quick.

### *4.1.3 Model description*

The aim is to calculate the seismic wavefield resulting from pressure fluctuations in a volcanic conduit. The conduit is cylindrical, (partially) filled with viscous fluid, orientated vertically and embedded in an infinite elastic solid [Fig. 4.1]. Both media are assumed to be homogeneous and isotropic which allows the P-SV and SH problems to be dealt with independently. The SH problem is not considered here since there is no obvious way to generate SH waves with this geometry. The symbols used in this chapter are listed in table 4.1 (below).

| **Symbol** | **Description** | **Reference** |
|---|---|---|
| $r$ | Radial coordinate | |
| $z$ | Vertical coordinate | |
| $t$ | Time | |
| $g$ | Gravity, 9.8 m/s | |
| $l$ | Conduit length | |
| $\pi$ | 3.1415927 | |
| $i$ | Square root of -1 | |
| $\rho$ | Density | Equation 4-23 |
| $\phi$ | P wave displacement potential | Equation 4-1 |
| $\Psi$ | Vector SV wave displacement potential | Equation 4-2 |
| $\psi$ | Scalar SV wave displacement potential | Equation 4-3 |
| $\mathbf{k}$ | Wavenumber vector | Section 4.2.1 |
| $k_z$ | Vertical component of wavenumber vector | Equation 4-5 |
| $e_\theta$ | Unit vector in $\theta$ direction | Equation 4-3 |
| $\omega$ | Angular frequency | |

| | | |
|---|---|---|
| $\alpha$ | P wave speed | |
| $\beta$ | S wave speed | |
| $K_0$, $K_1$ | Modified Bessel functions of first kind, of orders 0 and 1 | |
| $I_0$, $I_1$ | Modified Bessel functions of second kind, of orders 0 and 1 | |
| $l_p$ | Radial wavenumber for P waves | Equation 4-7 |
| $l_s$ | Radial wavenumber for S waves | Equation 4-8 |
| *A, B* | Coefficients of the P wave equation | Equations 4-5 |
| *C, D* | Coefficients of the S wave equation | Equations 4-6 |
| *v* | Vertical phase velocity (or magma rise speed) | Equation 4-12 |
| **u** | Displacement | Section 4.2.3 |
| $u_r$ | Radial displacement | Equation 4-14 |
| $u_z$ | Vertical displacement | Equation 4-14 |
| $\lambda$, $\mu$ | Lame (elastic) parameters. $\lambda$ is also used for wavelength. | Equation 4-17 |
| $r_0$ | Radial coordinate of conduit wall | Section 4.3.1 |
| $\Delta P$ | Presure perturbation | Equation 4-43 |
| $\Delta\tau$ | Shear stress perturbation | Eqaution 4-4-4 |
| *L* | Source separation along *z*-axis | Equation 4-49 |
| $\mathbf{u_s}$ | Displacement at seismometer | Equation 4-57 |
| $\Delta V$ | Change in volume | Equation 4-61 |
| $\kappa_s$ | Incompressibility of solid | Equation 4-63 |
| $B(t)_{t_1}^{t_2}$ | Boxcar function from $t_0$ to $t_1$ | Appendix E |
| $H(t-t_o)$ | Heaviside (step) function at $t_0$ | Appendix E |

**Table 4.1:** List of symbols used in Chapter 4.

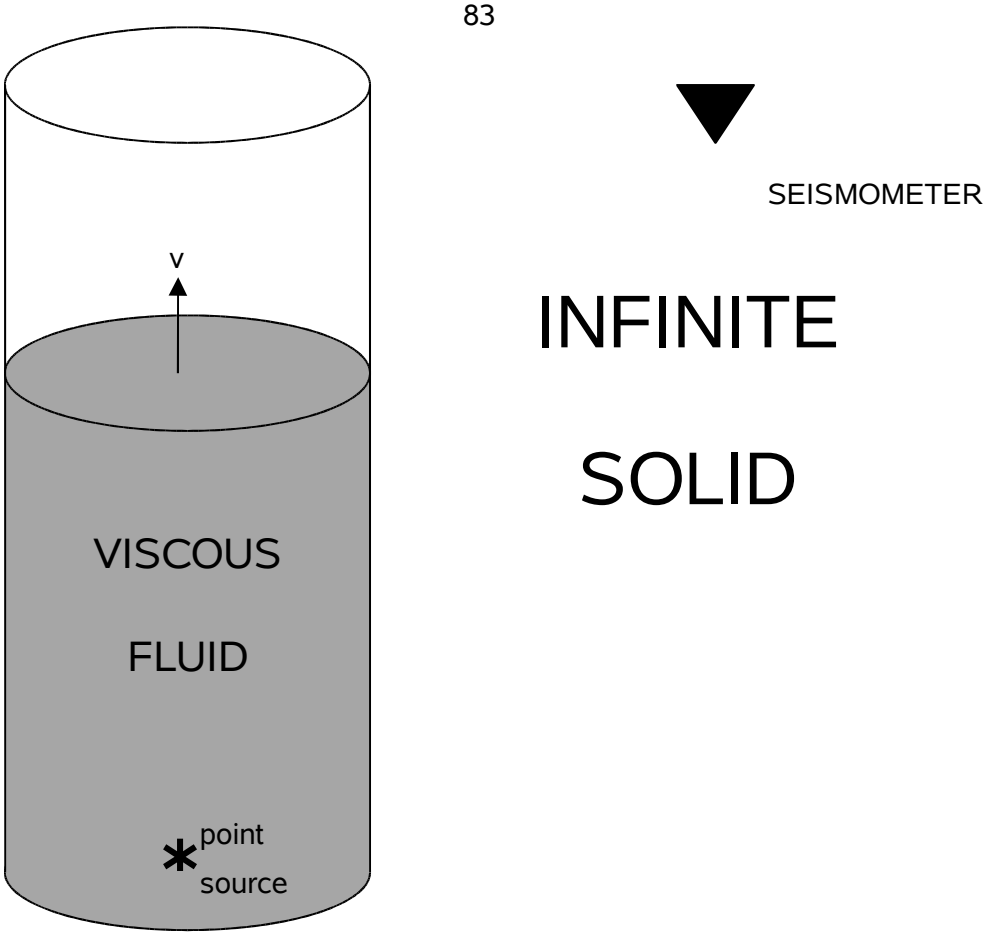


**Figure 4.1:** The technique assumes a cylindrical, vertical oriented conduit, partially filled with viscous magma. The magma may be rising with some speed v, in which case the distribution of pressure and shear stress forces along the conduit wall will change with time. Pressure forces, which act radially, generate P waves; shear stress forces act vertically downwards and generate SV waves. Alternatively, there may be a source in the fluid - which could arise from explosive degassing. This generates inhomogeneous P and S waves at the conduit wall leaking into the elastic solid.

# 4.2 P-SV wavefield

## *4.2.1 Solution of the wave equation in cylindrical co-ordinates*

In order to derive expressions for the displacement and stress in cylindrical co-ordinates it is necessary to solve the wave equation. The scalar wave equation for P waves in cylindrical co-ordinates is:

$$\phi_{:rr} + \frac{1}{r}\phi_{:r} + \phi_{:zz} = \frac{1}{\alpha^2}\phi_{:tt} \qquad \textbf{(4-1)}$$

where the P wave displacement potential $\phi = \phi(r,z,t)$ and $\alpha$ is the P wave speed.

The vector wave equation for S waves in cylindrical co-ordinates is:

$$\Psi_{:rr} + \frac{1}{r}\Psi_{:r} + \frac{1}{r^2}\Psi_{:\theta\theta} + \Psi_{:zz} = \frac{1}{\beta^2}\Psi_{:tt} \qquad \textbf{(4-2)}$$

where $\beta$ is the S wave speed and the SV wave displacement potential is:

$$\Psi(r,\theta,z,t) = \psi(r,z,t)\mathbf{e}_\theta \qquad \textbf{(4-3)}$$

Here $\psi(r,z,t)$ is the scalar SV displacement potential and $\mathbf{e}_\theta$ is the unit vector in the direction perpendicular to wave propagation (described by wavenumber **k**) and particle motion. But $\mathbf{e}_{\theta:\theta\theta} = -\mathbf{e}_\theta$, which gives:

$$\psi_{:rr} + \frac{1}{r}\psi_{:r} - \frac{1}{r^2}\psi + \psi_{:zz} = \frac{1}{\beta^2}\psi_{:tt} \qquad \textbf{(4-4)}$$

Solutions to 4-1 and 4-4 in the $k_z$-$\omega$ domain are respectively [Appendix A]:

$$\phi(r,k_z,\omega) = AK_0(l_p r) + BI_0(l_p r) \qquad \textbf{(4-5)}$$

$$\psi(r,k_z,\omega) = CK_1(l_s r) + DI_1(l_s r). \qquad \textbf{(4-6)}$$

where radial wavenumbers $l_p$ and $l_s$ are given by:

$$l_p^2 = k_z^2 - \frac{\omega^2}{\alpha^2} \quad \textbf{(4-7)}$$

$$l_s^2 = k_z^2 - \frac{\omega^2}{\beta^2} \quad \textbf{(4-8)}$$

and $K_n$ and $I_n$ are the *n*th order modified Bessel functions. (Only modified Bessel functions are used because normal Bessel functions describe inhomogeneous waves). The two-dimensional Fourier transform of $f(k_z,\omega)$ is given by:

$$f(z,t) = \frac{1}{2\pi}\int_{-\infty}^{\infty}\left(\frac{1}{2\pi}\int_{-\infty}^{\infty} f(k_z,\omega)e^{-ik_z z}\,dk_z\right)e^{i\omega t}\,d\omega\,. \qquad \textbf{(4-9)}$$

For convenience a shorthand notation is adopted such that 4-5 and 4-6 become respectively:

$$\phi(r,k_z,\omega) = AK_{0p} + BI_{0p} \qquad \textbf{(4-10)}$$

$$\psi(r,k_z,\omega) = CK_{1s} + DI_{1s} \qquad \textbf{(4-11)}$$

the additional subscript on the Bessel function indicates which radial wavenumber (P or S wave) the Bessel function operates on. For the P wave (Bessel functions with a subscript *p*) the argument of the Bessel function is $l_p r$. For the S wave (Bessel functions with a subscript *s*) the argument of the Bessel function is $l_s r$.

### *4.2.2 Physical interpretation of solutions to wave equation*

The wave equation solutions in 4-10 and 4-11 can be thought of as describing the wavefield in terms of an infinite sum of plane waves propagating out from the origin at all wavelengths and at all angles. This is because 4-5 and 4-6 are approximately the mathematical expression of a plane wave.

By summing over all frequencies for constant vertical wavenumber, the radial wavenumber expressed in 4-7 and 4-8 changes, i.e. the direction of plane wave propagation changes. By summing over all frequencies and all vertical wavenumbers, the phase speed of the plane wave takes all values too. Phase speed is given by:

$$v = \pm \frac{\omega}{k_z} \qquad \textbf{(4-12)}$$

The superposition of these waves results in spherical waves, which means near-field effects can be accounted for. [See Appendix B for more details].

### 4.2.3 Near field effects

At Stromboli in 1992 and 1995 the seismic stations were less than 1 wavelength from the source region for frequencies below ~ 1Hz, so it is necessary to model near-field effects. (Some modelling methods include only far field effects, and others only near field effects, e.g. the Mogi model). To include both the solution is decomposed into an infinite sum over plane waves (i.e. by integration). Therefore an infinite number of far field problems are solved, which are simple, rather than solve the near field problem directly. In practice a finite number of far field problems are solved (by adjusting the limits of integration) - the more included, the more accurately that near field terms are accounted for.

### 4.2.4 Displacement

Continuity of displacement is one of the boundary conditions which applies in this model. In order to use that boundary condition, an expression for displacement, **u** (*r,z,t*), in terms of P and SV wave potentials in cylindrical co-ordinates must be derived. Displacement in an infinite homogeneous space is given by:

$$\mathbf{u}(r,z,t) = \nabla\phi + \nabla \times \Psi \qquad \textbf{(4-13)}$$

where $\phi$ is the scalar P-wave potential, and $\Psi=\psi e_\theta$ is the vector SV-wave potential in the axially-symmetric case. Hence **u** may be written as:

$$\mathbf{u}(r,z,t) = \left[u_r(r,z,t), 0, u_z(r,z,t)\right] = \left[\phi_{;r} - \psi_{;z}, 0, \phi_{;z} + \psi_{;r} + \psi\, r^{-1}\right] \qquad \textbf{(4-14)}$$

Now using the following relations for derivatives of the modified Bessel functions, $K_0$, $K_1$, $I_0$ and $I_1$ [Appendix C] and equations 4-10 and 4-11 the derivatives in 4-14 can be expressed in terms of coefficients *A, B, C* and *D* as:

$$\phi_{;r}(r,k_z,\omega) = l_p\left(BI_{1p} - AK_{1p}\right)$$
$$\phi_{;z}(r,k_z,\omega) = -ik_z\left(AK_{0p} + BI_{0p}\right)$$
$$\psi_{;r}(r,k_z,\omega) = D\left(l_s I_{0s} - I_{1s} r^{-1}\right) - C\left(l_s K_{0s} + K_{1s} r^{-1}\right)$$
$$\psi_{;z}(r,k_z,\omega) = -ik_z\left(CK_{1s} + DI_{1s}\right)$$

Hence 4-14 can be expressed in components as:

$$u_r(r,k_z,\omega) = -l_p(AK_{1p} - BI_{1p}) + ik_z(CK_{1s} + DI_{1s}) \qquad \textbf{(4-15)}$$

$$u_z(r,k_z,\omega) = -ik_z(AK_{0p} + BI_{0p}) + l_s(DI_{0s} - CK_{0s}) \qquad \textbf{(4-16)}$$

### *4.2.5 Stress*

Continuity of stress is a boundary condition for this model. In order to apply this, expressions for stress components in terms of P and SV wave potentials must be derived. When axial symmetry holds the only non-zero components of the stress tensor are $\sigma_{rr}$ (normal stress),$\sigma_{rz}$ (shear stress), $\sigma_{\theta\theta}$ and $\sigma_{zz}$. In the P-SV problem only the first two are constrained. For an elastic medium these are (Hooke's Law):

$$\sigma_{rr} = \lambda\,(\nabla.\mathbf{u}) + 2\mu\, e_{rr} \qquad \textbf{(4-17)}$$

$$\sigma_{rz} = 2\mu\, e_{rz} \qquad \textbf{(4-18)}$$

where $e_{rr}$ and $e_{rz}$ are components of the strain tensor and $\lambda$ and $\mu$ are the Lamé parameters. Expressing these in terms of displacement gives:

$$\sigma_{rr} = \lambda\,(u_{r;r} + u_r r^{-1} + u_{z;z}) + 2\mu\, u_{r;r} \qquad \textbf{(4-19)}$$

$$\sigma_{rz} = \mu\,(u_{r;z} + u_{z;r}) \qquad \textbf{(4-20)}$$

Expressing these in terms of P and S wave potentials by using 4-14 gives:

$$\sigma_{rr} = \lambda\left(\phi_{;rr} + \phi_{;r} r^{-1} + \phi_{;zz}\right) + 2\mu\left(\phi_{;rr} - \psi_{;rz}\right) \qquad \textbf{(4-21)}$$

$$\sigma_{rz} = \mu \left( 2\phi_{;rz} - \psi_{;zz} + \psi_{;rr} - \psi\, r^{-2} + \psi_{;r} r^{-1} \right) \quad \textbf{(4-22)}$$

Then using the relations:

$$\lambda + 2\mu = \rho\alpha^{2} \qquad \textbf{(4-23)}$$

$$\mu = \rho\beta^{2} \qquad \textbf{(4-24)}$$

where $\rho$ is density, and $\alpha$ and $\beta$ are the P and S wave velocities respectively. It follows that:

$$\sigma_{rr} = \rho\alpha^{2} \left( \phi_{;rr} + \phi_{;r} r^{-1} + \phi_{;zz} \right) - 2\rho\beta^{2} \left( \phi_{;r} r^{-1} + \phi_{;zz} + \psi_{;rz} \right) \qquad \textbf{(4-25)}$$

$$\sigma_{rz} = \rho\beta^{2} \left( 2\phi_{;rz} - \psi_{;zz} + \psi_{;rr} - \psi\, r^{-2} + \psi_{;r} r^{-1} \right) \qquad \textbf{(4-26)}$$

Finally using the wave equations 4-1 and 4-4 to eliminate second derivatives w.r.t *r* gives:

$$\sigma_{rr} = \rho\left( \phi_{;tt} - 2\beta^{2} \left( \phi_{;r} r^{-1} + \phi_{;zz} + \psi_{;rz} \right) \right) \qquad \textbf{(4-27)}$$

$$\sigma_{rz} = \rho\left( \psi_{;tt} + 2\beta^{2} \left( \phi_{;rz} - \psi_{;zz} \right) \right) \qquad \textbf{(4-28)}$$

Now substituting for derivatives of $K_0$, $K_1$, $I_0$ and $I_1$ [Appendix C], and using 4-10 and 4-11, each of the terms in 4-27 and 4-28 can be expressed in terms of coefficients *A, B, C* and *D*:

$$\phi_{;tt}(r, k_z, \omega) = -\omega^{2}\left( AK_{0p} + BI_{0p} \right)$$
$$\phi_{;r}(r, k_z, \omega) = l_p\left( BI_{1p} - AK_{1p} \right)$$
$$\phi_{;zz}(r, k_z, \omega) = -k_z^{2}\left( AK_{0p} + BI_{0p} \right)$$
$$\phi_{;rz}(r, k_z, \omega) = -ik_z l_p\left( BI_{1p} - AK_{1p} \right)$$
$$\psi_{;rz}(r, k_z, \omega) = -ik_z\left( D\left( l_s I_{0s} - I_{1s} r^{-1} \right) - C\left( l_s K_{0s} + K_{1s} r^{-1} \right) \right)$$
$$\psi_{;tt}(r, k_z, \omega) = -\omega^{2}\left( CK_{1s} + DI_{1s} \right)$$
$$\psi_{;zz}(r, k_z, \omega) = -k_z^{2}\left( CK_{1s} + DI_{1s} \right)$$

Hence 4-27 and 4-28 become:

$$\sigma_{rr}(r,k_z,\omega)\mu^{-1} = (2k_z^2 - \omega^2\beta^{-2})(AK_{0p} + BI_{0p}) + 2l_p r^{-1}(AK_{1p} - BI_{1p}) - 2ik_z\left(C(l_s K_{0s} + K_{1s} r^{-1}) - D(l_s I_{0s} - I_{1s} r^{-1})\right) \quad \textbf{(4-29)}$$

$$\sigma_{rz}(r,k_z,\omega)\mu^{-1} = (2k_z^2 - \omega^2\beta^{-2})(CK_{1s} + DI_{1s}) + 2ik_z l_p (AK_{1p} - BI_{1p}) \quad \textbf{(4-30)}$$

The stress components in their most useful form are obtained by replacing $\omega$ using 4-8:

$$\sigma_{rr}(r,k_z,\omega)\mu^{-1} = (k_z^2 + l_s^2)(AK_{0p} + BI_{0p}) + 2l_p r^{-1}(AK_{1p} - BI_{1p}) - 2ik_z\left(C(K_{1s} r^{-1} + l_s K_{0s}) + D(I_{1s} r^{-1} - l_s I_{0s})\right) \quad \textbf{(4-31)}$$

$$\sigma_{rz}(r,k_z,\omega)\mu^{-1} = (k_z^2 + l_s^2)(CK_{1s} + DI_{1s}) + 2ik_z l_p (AK_{1p} - BI_{1p}) \quad \textbf{(4-32)}$$

### *4.2.6 Displacement and stress in the fluid*

Since the fluid is viscous, P and SV waves can propagate within it. Using 4-15, 4-16, 4-31 and 4-32 the displacement and stress components in the fluid can be written as:

$$u_{rf}(r,k_z,\omega) = -l_{pf}(A_f K_{1pf} - B_f I_{1pf}) + ik_z(C_f K_{1sf} + D_f I_{1sf}) \quad \textbf{(4-33)}$$

$$u_{zf}(r,k_z,\omega) = -ik_z(A_f K_{0pf} + B_f I_{0pf}) + l_{sf}(D_f I_{0sf} - C_f K_{0sf}) \quad \textbf{(4-34)}$$

$$\sigma_{rrf}(r,k_z,\omega)\mu_f^{-1} = (k_z^2 + l_{sf}^2)(A_f K_{0pf} + B_f I_{0pf}) + 2l_{pf} r^{-1}(A_f K_{1pf} - B_f I_{1pf}) - 2ik_z\left(C_f(K_{1sf} r^{-1} + l_{sf} K_{0sf}) + D_f(I_{1sf} r^{-1} - l_{sf} I_{0sf})\right) \quad \textbf{(4-35)}$$

$$\sigma_{rzf}(r,k_z,\omega)\mu_f^{-1} = (k_z^2 + l_{sf}^2)(C_f K_{1sf} + D_f I_{1sf}) - 2ik_z l_{pf}(A_f K_{1pf} - B_f I_{1pf}) \quad \textbf{(4-36)}$$

where the extra subscript *f* denotes parameters of the fluid.

### 4.2.7 Displacement and stress in the solid

The displacement and stress components in the solid can be written as:

$$u_{rs}(r,k_z,\omega) = -l_{ps}(A_s K_{1ps} - B_s I_{1ps}) + ik_z(C_s K_{1ss} + D_s I_{1ss}) \quad \textbf{(4-37)}$$

$$u_{zs}(r,k_z,\omega) = -ik_z(A_s K_{0ps} + B_s I_{0ps}) + l_{ss}(D_s I_{0ss} - C_s K_{0ss}) \quad \textbf{(4-38)}$$

$$\begin{aligned}\sigma_{rrs}(r,k_z,\omega)\mu_s^{-1} &= (k_z^2 + l_{ss}^2)(A_s K_{0ps} + B_s I_{0ps}) + 2l_{ps}r^{-1}(A_s K_{1ps} - B_s I_{1ps}) \\ &\quad - 2ik_z\left(C_s(K_{1s}r^{-1} + l_{ss}K_{0ss}) + D_s(I_{1ss}r^{-1} - l_{ss}I_{0ss})\right)\end{aligned} \quad \textbf{(4-39)}$$

$$\sigma_{rzs}(r,k_z,\omega)\mu_s^{-1} = (k_z^2 + l_{ss}^2)(C_s K_{1ss} + D_s I_{1ss}) + 2ik_z l_{ps}(A_s K_{1ps} - B_s I_{1ps}) \quad \textbf{(4-40)}$$

where the extra subscript *s* denotes parameters of the solid.

## 4.3 Infinite solid

### 4.3.1 Boundary conditions at the conduit wall

This is the case considered by *Theisse* [1996]. There must be continuity of displacement and stress at the conduit wall, $r=r_0$. This is true, even for shear components, since there can be no slip on a boundary between a viscous fluid and a solid. In the P-SV problem this gives four equations:

$$u_{rf}(r_0) = u_{rs}(r_0) \quad \textbf{(4-41)}$$

$$u_{zf}(r_0) = u_{zs}(r_0) \quad \textbf{(4-42)}$$

$$\sigma_{rrf}(r_0) = \sigma_{rrs}(r_0) + \Delta P \quad \textbf{(4-43)}$$

$$\sigma_{rzf}(r_0) = \sigma_{rzs}(r_0) - \Delta\tau \quad \textbf{(4-44)}$$

where $\Delta P(a,z,t)$ and $\Delta\tau(a,z,t)$ are perturbations to the normal pressure field and shear stress field, respectively.

The boundary conditions 4-41 to 4-44 must now be written in terms of the coefficients $A_f$, $B_f$, $C_f$, $D_f$, $A_s$, $B_s$, $C_s$ and $D_s$ since these must be determined in order to calculate synthetic seismograms. Solutions of the wave equation which include $I_0$ and $I_1$ cannot exist in the unbounded solid, since these functions behave exponentially for large $r$, which is not physically meaningful (however they can be used in the fluid since that is bounded in the radial direction). Hence the coefficients $B_s$ and $D_s$ , in 4-37 to 4-40, must be zero. Similarly $K_0$ and $K_1$ tend towards infinity as $r$ decreases, which means that $A_f$ and $C_f$ can only be used to represent sources in the fluid. Physically $A_f$ represents a P wave point source, and $C_f$ represents an S wave point source, at the origin. These sources are known inputs into the model. Shear failure within the viscous fluid is not considered here, so S wave sources are not considered (these are eliminated by setting $C_f$=0; see Appendix D for more on the behaviour of the modified Bessel functions). The upshot is that four equations in four unknowns remain.

These four simultaneous equations can now written in matrix form $\underline{\underline{\mathbf{A}}}\mathbf{x}=\mathbf{d}+\mathbf{y}$, with (known) source terms on the right, and the unknown coefficients (the vector **x**) on the left:

$$\underline{\underline{\mathbf{A}}} \qquad \mathbf{x} \qquad \mathbf{d} \qquad \mathbf{y}$$

$$\begin{pmatrix} a_{11} & a_{12} & a_{13} & a_{14} \\ a_{21} & a_{22} & a_{23} & a_{24} \\ a_{31} & a_{32} & a_{33} & a_{34} \\ a_{41} & a_{42} & a_{43} & a_{44} \end{pmatrix} \begin{pmatrix} A_s \\ B_f \\ C_s \\ D_f \end{pmatrix} = \begin{pmatrix} 0 \\ 0 \\ \Delta P \\ -\Delta\tau \end{pmatrix} + \begin{pmatrix} y_1 \\ y_2 \\ y_3 \\ y_4 \end{pmatrix} A_f \qquad \textbf{(4-45)}$$

The matrix $\underline{\underline{\mathbf{A}}}$ and vector **y** come from combining the relations for displacement and stress in the fluid (4-33 to 4-36) and in the solid (4-37 to 4-40) with the boundary conditions above (4-41 to 4-44) noting that $B_s$=$D_s$=$C_f$=0. The source terms, vectors **d** and **y**, are discussed in section 4.4. Explicity this matrix equation is:

$$\begin{pmatrix} l_{ps}K_{1ps} & l_{pf}I_{1pf} & -ik_zK_{1ss} & ik_zI_{1sf} \\ ik_zK_{0ps} & -ik_zI_{0pf} & l_{ss}K_{0ss} & l_{sf}I_{0sf} \\ -\mu_s\left((k_z^2+l_{ss}^2)K_{0ps}+2l_{ps}K_{1ps}r_0^{-1}\right) & \mu_f\left((k_z^2+l_{sf}^2)I_{0pf}-2l_{pf}I_{1pf}r_0^{-1}\right) & 2ik_z\mu_s\left(K_{1ss}r_0^{-1}+l_{ss}K_{0ss}\right) & -2ik_z\mu_f\left(I_{1sf}r_0^{-1}-l_{sf}I_{0sf}\right) \\ -2i\mu_s k_z l_{ps}K_{1ps} & -2i\mu_f k_z l_{pf}I_{1pf} & -\mu_s(k_z^2+l_{ss}^2)K_{1ss} & \mu_f(k_z^2+l_{sf}^2)I_{1sf} \end{pmatrix} \begin{pmatrix} A_s \\ B_f \\ C_s \\ D_f \end{pmatrix}$$

$$= \begin{pmatrix} l_{pf}K_{1pf} \\ ik_zK_{0pf} \\ -\mu_f\left((k_z^2+l_{sf}^2)K_{0pf}+2l_{pf}K_{1pf}r_0^{-1}\right) \\ -2ik_z\mu_f l_{pf}K_{1pf} \end{pmatrix} A_f + \begin{pmatrix} 0 \\ 0 \\ \Delta P \\ -\Delta\tau \end{pmatrix}$$

The aim is to find $\mathbf{x}=\underline{\underline{\mathbf{A}}}^{-1}(\mathbf{d}+\mathbf{y})$ by inversion using a computer. Once **x** is found, the coefficients $A_s$ and $C_s$ are known, so 4-37 and 4-38 can be used to calculate synthetic seismograms. This gives the solution for any given combination in the $k_z$-$\omega$ domain, but it is the solution in the *(z,t)* domain that is required. To get this, first note that by 4-9, the displacement in the solid, $\mathbf{u_s}(z,t)$, is given by:

$$\mathbf{u}_s(z,t) = \frac{1}{2\pi}\int_{-\infty}^{\infty}\left(\frac{1}{2\pi}\int_{-\infty}^{\infty}\mathbf{u}_s(k_z,\omega)e^{-ik_z z}dk_z\right)e^{i\omega t}d\omega\,, \qquad \textbf{(4-46)}$$

This is just a 2-dimensional Fourier transform. To evaluate this on a computer the continuous integrals must be replaced by a discrete sum. This is done by using the discrete wavenumber method.

## *4.3.2 Discrete wavenumber method*

The method of discrete wave numbers was first described by Bouchon and Aki [1977] and consists of a discretization of the Fourier transform and the introduction of complex frequencies.

The Fourier transform:

$$f(z,\omega) = \frac{1}{2\pi}\int_{-\infty}^{\infty} f(k_z,\omega)e^{-ik_z z}dk_z \qquad \textbf{(4-47)}$$

becomes:

$$f(z,\omega) = \frac{\delta k_z}{2\pi}\sum_{n=-N}^{N} f(k_n,\omega)e^{-ik_n z} \qquad \textbf{(4-48)}$$

The series is convergent with the number *N* being determined by trial and error. The effect of discretization in the wavenumber domain is to introduce periodic sources in space situated at a distance *L* apart along the *z*-axis where:

$$\delta k_z = \frac{2\pi}{L} \qquad \textbf{(4-49)}$$

These fictitious sources are not wanted. They can be removed from the solution altogether by making *L* so large that arrivals from even the closest fictitious source will not arrive until after the time window of interest. Such an approach is not always preferred because execution time can become very long. An alternative approach is to introduce a *constant* imaginary part to the frequency:

$$\omega = \omega_r - i\omega_i \; with \omega_i > 0 \qquad \textbf{(4-50)}$$

this has the effect of damping the (later) arrivals from the fictitious sources and so considerably reducing the problem of spatial aliasing. In addition, the singularities of $f(r,k_n,\omega)$ which lay on the real $k_z$-axis are now shifted into the 2nd and 4th quadrants [Appendix D] of the complex plane.

The introduction of a complex frequency also affects the time Fourier transform:

$$e^{i\omega t} = e^{i(\omega_r - i\omega_i)t} = e^{\omega_i t} e^{-i\omega_r t} \qquad \textbf{(4-51)}$$

This compensates for the attenuation of later arrivals already discussed. Hence the time Fourier transform:

$$f(z,t) = \frac{1}{2\pi} \int_{-\infty}^{\infty} f(z,\omega) e^{i\omega t} d\omega \qquad \textbf{(4-52)}$$

becomes:

$$f(z,t) = \frac{e^{\omega_i t}}{2\pi} \int_{-\infty}^{\infty} f(z,\omega) e^{i\omega_r t} d\omega_r \qquad \textbf{(4-53)}$$

For computational purposes this formula is replaced by its discrete form:

$$f(z,t_c) = \frac{e^{\omega_i t_c}}{2\pi}\delta\omega_m \sum_{m=-M}^{M} f(z,\omega_m)e^{i\omega_m t_c} \quad \textbf{(4-54)}$$

where:

$$t_c = \frac{2\pi c}{M\delta\omega_r} \quad \textbf{(4-55)}$$

and:

$$\omega_m = m\delta\omega_r \quad \textbf{(4-56)}$$

Hence 4-46 becomes:

$$\mathbf{u}_s(z,t_c) = \frac{e^{\omega_i t_c}}{2\pi}\delta\omega_m \sum_{m=-M}^{M}\left(\frac{\delta k_z}{2\pi}\sum_{n=-N}^{N}\mathbf{u}_s(k_z,\omega)e^{-ik_n z}\right)e^{i\omega_m t_c} \quad \textbf{(4-57)}$$

### *4.3.3 Summary and coding*

Synthetic seismograms are calculated by solving 4-57. In order to find $\mathbf{u_s}(k_z,\omega)$, the boundary conditions in the $(k_z,\omega)$-domain must first be solved in order to find the coefficients $A_s$ and $C_s$. $\mathbf{u_s}(z,\omega)$ is then formed by repeating this process for all $k_z$ of interest and summing the result. Practically the summation over frequencies can be performed by using an FFT which speeds the method up. The algorithm for the problem is then:

- Loop over angular frequency ω
    - ◊ Loop over vertical-wavenumber $k_z$
        - ⇒ Calculate matrix $\underline{\underline{\mathbf{A}}}$ [equation 4.45] for this $(k_z,\omega)$.
        - ⇒ Calculate source vectors **d** and **y** [section 4.4] for this $(k_z,\omega)$.
        - ⇒ Invert matrix equation 4.45 - this is the matrix equation for boundary conditions at the conduit wall - to yield vector **x** of coefficients.
        - ⇒ Calculate $\mathbf{u_s}(k_z,\omega)$ at $r_s$=radial distance of seismometer from source using 4-37 and 4-38.

⇒ Multiply by exp(-ik$_z$z) $\delta k_z/2\pi$ and add to $\mathbf{u_s}(z,\omega)$ - [equation 4-57].

◊ End loop

- End loop
- Use FFT to derive $\mathbf{u_s}(z,t)$ from $\mathbf{u_s}(z,\omega)$ - [equation 4-57].

The codes were written in Fortran 77 on a Unix workstation.

# 4.4 Sources

## *4.4.1 Source vectors*

Sources are described through vectors **d** and **y** in equation 4-45:

$$\begin{pmatrix} l_{ps}K_{1ps} & l_{pf}I_{1pf} & -ik_zK_{1ss} & ik_zI_{1sf} \\ ik_zK_{0ps} & -ik_zI_{0pf} & l_{ss}K_{0ss} & l_{sf}I_{0sf} \\ -\mu_s\left((k_z^2+l_{ss}^2)K_{0ps}+2l_{ps}K_{1ps}r_0^{-1}\right) & \mu_f\left((k_z^2+l_{sf}^2)I_{0pf}-2l_{pf}I_{1pf}r_0^{-1}\right) & 2ik_z\mu_s\left(K_{1ss}r_0^{-1}+l_{ss}K_{0ss}\right) & -2ik_z\mu_f\left(I_{1sf}r_0^{-1}-l_{sf}I_{0sf}\right) \\ -2i\mu_s k_z l_{ps}K_{1ps} & -2i\mu_f k_z l_{pf}I_{1pf} & -\mu_s(k_z^2+l_{ss}^2)K_{1ss} & \mu_f(k_z^2+l_{sf}^2)I_{1sf} \end{pmatrix} \begin{pmatrix} A_s \\ B_f \\ C_s \\ D_f \end{pmatrix}$$

$$= \begin{pmatrix} l_{pf}K_{1pf} \\ ik_zK_{0pf} \\ -\mu_f\left((k_z^2+l_{sf}^2)K_{0pf}+2l_{pf}K_{1pf}r_0^{-1}\right) \\ -2ik_z\mu_f l_{pf}K_{1pf} \end{pmatrix} A_f + \begin{pmatrix} 0 \\ 0 \\ \Delta P \\ -\Delta\tau \end{pmatrix} = \mathbf{y}A_f + \mathbf{d}$$

**(4-45)**

The coefficient $A_f$ describes point sources at the origin in the fluid. A point source can be used to represent a pressure change within a spherical region in the fluid; e.g the growth of a bubble, explosive degassing in section of the conduit, or pressurisation of a spherical magma body.

Perturbations $\Delta P$ and $\Delta\tau$ can be used to describe moving sources and extended sources. These variables are used to model magma rising in the conduit and the pressure changes due to bubbles rising in the conduit.

In the following sections, first point sources, and then extended sources, are examined in more detail.

### 4.4.2 Point sources

Consider:

$$\phi_f(r,z,t) = \int_{-\infty}^{\infty}\int_{-\infty}^{\infty}\left(A_f K_0(l_{pf} r) + B_f I_0(l_{pf} r)\right)e^{i(k_z z-\omega t)}dk_z\,d\omega \qquad \textbf{(4-58)}$$

which is the displacement potential for P waves in the fluid. It consists of two parts, the first of which describes the source potential - this is the term containing $K_0$ since that becomes singular at $r$=0 and therefore represents a source:

$$\phi_{source}(r,z,t) = \int_{-\infty}^{\infty}\int_{-\infty}^{\infty} A_f K_0(l_{pf} r)e^{i(k_z z-\omega t)}dk_z\,d\omega \qquad \textbf{(4-59)}$$

If $A_f$ is independent of $k_z$ and $\omega$, then 4-59 is just a sum over plane waves travelling in different directions at different speeds. The interference of these waves leads to spherical wavefronts, i.e. representing a point source.

If $A_f$ is a function of frequency, but not of $k_z$, then 4-59 still represents a point source, but with a time variation given by:

$$a(t) = \int_{-\infty}^{\infty} A_f(\omega)e^{-i\omega t}d\omega \qquad \textbf{(4-60)}$$

Physically $A_f$ is related to the volume change, $\Delta V$, in the source region. Following the definition of the Fourier transforms established in this thesis, $A_f$ is just:

$$A_f(\omega) = \frac{\Delta V(\omega)}{2\pi}. \qquad \textbf{(4-61)}$$

In practice, the way to use this type of source is to choose $\Delta V(t)$, and then calculate $A_f(\omega)$ using:

$$A_f(\omega) = \frac{1}{2\pi}\int_{-\infty}^{\infty} \Delta V(t) e^{i\omega t} dt \qquad \textbf{(4-62)}$$

This is then substituted into the matrix equation 4-45. However, because there is no anisotropy or attenuation in the model, the seismograms produced, **u**(*t*), will be proportional to the volume change, $\Delta V(t)$ - i.e. the ground motion observed at any station will have the same waveform as the source signature (for P and S wave propagation times which are small compared to the period of the waves being considered). Since there is nothing to be learned by using complicated source functions, only delta pulses and step functions will be considered.

In order for the source region to expand by an amount $\Delta V$, work must be done by some force. This force is provided by a rise in pressure, $\Delta P$, acting over the surface area of the source region [Fig. 4.2]. A fundamental expression relating $\Delta V$ and $\Delta P$ is:

$$\Delta P = -\kappa_s \frac{\Delta V}{V_0}. \qquad \textbf{(4-63)}$$

where $\kappa_s$ is the incompressibility of the solid. Note that it is the incompressibility of the solid, not the fluid, that matters here, since the pressure forces in the fluid must compress the solid. This allows us to compare the likelihood of point sources and extended sources based on the pressure changes required to produce a particular observation.

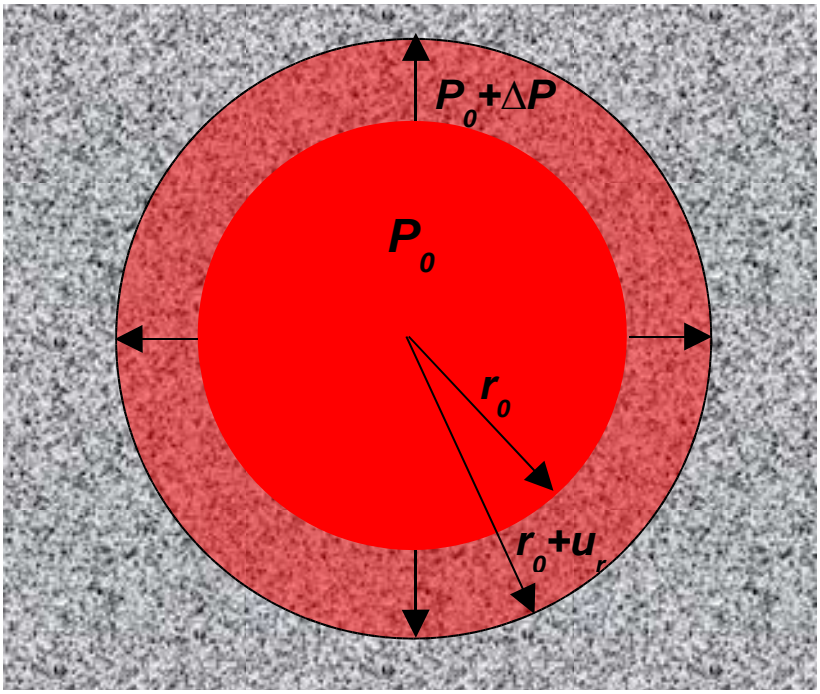

**Figure 4.2:** In order for a spherical magma body to increase its radius by $u_r(r_0)$ (the radial displacement at the interface between magma and rock), some force must do work to compress the surrounding solid. This force is provided by a pressure change $\Delta P$ acting over the surface of the sphere.

A point source can be used to describe a process known as *explosive degassing*. This can occur during from the ascent of magma. The magma contains volatiles which are dissolved at great depth, principally carbon dioxide and water. As the mixture ascends, the pressure diminishes as does the solubility in the magma of these volatiles. When the solubility becomes less than the concentration of volatiles, magma and gas separate to form two distinct phases. If magma rises more quickly than phases can separate, the difference between solubility and concentration increases, resulting in explosive degassing.

### 4.4.3 Moving point sources

In order to model a moving point source (which will be used later to model a rising bubble/slug flow), point source models can be calculated at different depths. These can then be staggered uniformly in time to represent a source which moves with a constant velocity, or by using shorter and shorter intervals of time, a source which accelerates as it nears the surface can be simulated.

### 4.4.4 Extended sources

The long period signals observed prior to eruptions at Stromboli [*Neuberg and Luckett*, 1996] and Aso [*Kaneshima et al*., 1996] may indicate:

1. injection of magma into the base of a magma chamber,
2. magma rising through a conduit to the surface, or
3. the pressurization of a conduit section.

It is not clear that any point source models could be used to represent such sources. Extended sources will be described by the changes in pressure, $\Delta P$, and shear stress, $\Delta\tau$, they produce at the conduit wall.

Four mechanisms are considered for producing pressure changes in these source models:

1. Advective overpressure, which is the result of bubbles rising within a sealed conduit [*Sahagian and Proussevitch*, 1992]. This mechanism requires the conduit to be sealed and the walls to be rigid. In this thesis, advective overpressure is considered as a mechanism for increasing the pressure in a static magma column, leading to fracture of a cap rock. The rapid decompression of the magma may cause explosive degassing and expansion of the mix, observable as a gas-driven eruption.

2. The pressure gradient that comes from the weight of overlying magma within the conduit. As magma rises (or falls) in a conduit the height of the magma column changes which leads to pressure changes along the entire conduit wall. For a basaltic magma, the pressure gradient deviates very little from lithostatic.

3. The overpressure arises because the magma/gas mixture rises more quickly than it can expand. Even if the overpressure remains constant, pressure changes will occur along the conduit wall as rising magma displaces lower pressure gas above it.

4. The dynamic pressure of a moving fluid which is described by Bernoulli's equation; this is equivalent to an underpressure [Section 4.4.9] and so it can be modelled in the same way as an overpressure.

In the source models that follow, advective overpressure for a static magma column (with rising bubbles) is first considered. Then a rising (moving) magma source is studied; this has a constant pressure gradient, a dynamic pressure, and an optional overpressure [Fig. 4.3]. For a rising magma shear stress must also be considered.

In order to model a particular source, expressions for $\Delta P(z,t)$ and $\Delta\tau(z,t)$ at the conduit wall must be deduced, and then transformed into the $(k_z,\omega)$-domain. In the following sections expressions for several volcanic sources are derived. In all of these models, a cylindrical, vertically oriented conduit is assumed.

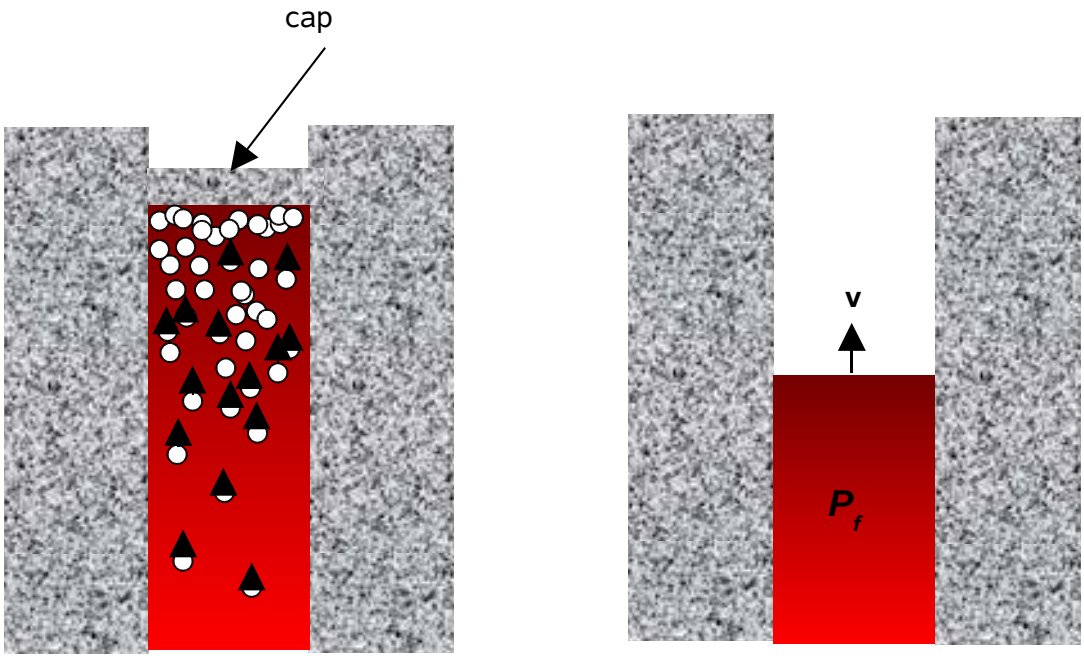


(a) Advective overpressure

(b) Rising magma

$$P_f = P_0 + P_{over} + P_{grad} - P_d$$

**Figure 4.3:** Mechanisms for causing pressure changes along the conduit walls (a) Advective overpressure is the mechanism whereby rising bubbles lead to increased pressure throughout the magma column. This mechanism requires that the conduit is sealed and that bubbles are not reabsorbed by the magma as pressure increases. (b) For rising magma there are four components to the pressure field: $P_0$ is atmospheric pressure, $P_{over}$ is overpressure in the fluid (assumed constant with depth), $P_{grad}(z)$ is the pressure gradient, which must exist in order for the magma to rise, and $P_d$ is the dynamic pressure which is described by the Bernoulli equation.

### *4.4.5 Advective overpressure*

The simplest kind of extended source is a line source. In a volcanic context such a source can represent the pressurization of a sealed section of conduit in response to rising bubbles. In the model of *Sahagian and Proussevitch* [1992], a bubble rising a height $z$ in the conduit raises the overall pressure throughout the conduit by $\rho gz$, where $\rho$ is fluid density and $g$ is the acceleration due to gravity. Their model

assumed that the conduit was sealed and rigid, and that no re-absorption of the bubble would occur as the pressure increased. These assumptions are not realistic for a volcano, but such a mechanism may increase the pressure in the conduit, with somewhat reduced efficiency, though experimental data are needed to verify this.

In this model the pressure increases until it exceeds the yield strength of the cap rock sealing the conduit, resulting in rapid expansion of the bubbles which have accumulated beneath this cap. A choked-flow regime would probably occur because of the relatively small vent size, and the decompression would occur over several passages of a rarefaction wave down and up the conduit [*Kieffer and Sturtevant*, 1984].

Bubbles are assumed to rise at a constant rate, and so the pressure in the system also changes at a steady rate (*dP/dt* is constant). At time $t_{max}$ the cap fails and the pressure in the conduit instantaneously drops to zero. Since there is no movement of magma in this model, there is no shear stress.

The first task is to write down an expression for $\Delta P(z,t)$. The total pressure change for times between $t=0$ and $t=t_{max}$ is the product of $t$ with $dP/dt$. This only applies to points for which $0<z<l$ i.e. the region inside the conduit ($z=0$ corresponds to the base of the conduit, $l$ is conduit length). The limits on $t$ and $z$ are represented mathematically by Boxcar functions (Appendix E), and so $\Delta P(z,t)$ can be written thus

$$\Delta P(z,t) = \frac{dP}{dt} tB(t)_0^{t_{\max}} B(z)_0^{l} . \qquad \textbf{(4-64)}$$

This is transformed into the $(k_z,\omega)$-domain by using E-9 and E-12:

$$\Delta P(k_z,\omega) = \frac{dP}{dt}\left\{\frac{e^{-i\omega t_{\max}}(1+i\omega t_{\max})-1}{\omega^2}\right\}\frac{e^{ik_z l}-1}{ik_z} \qquad \textbf{(4-65)}$$

A constant rate of change of pressure is assumed because nothing can be learned from forcing *dP/dt* to match the waveform observed in a particular seismogram, since the variation in pressure could not itself be accounted for.

### 4.4.6 Rising magma as a seismic source

As viscous magma rises up the vertical conduit, the spatial distribution of pressure and shear stress on the conduit wall changes with time [Fig. 3.10]. Pressure exerts a force normal to the conduit wall, shear stress exerts a force which is directed vertically downwards. There is always a pressure gradient in any magma column, arising from the weight of overlying magma (and rock if the conduit is sealed). A rising magma will also experience a dynamic pressure, given by the Bernoulli equation. Finally it may have an overpressure, because it has risen too quickly to stabilize with the lithostatic pressure gradient. In the following sections each of these components is explored separately. Superposition can then be used to model any rising magma source.

These various sources of pressure change can be summarised as:

$$P_{fluid}(z) - P_{atmosphere} = \rho g(h - z) + P_{overpressure} + P_{dynamic} \quad \textbf{(4-66)}$$

It expresses the difference between fluid pressure and atmospheric pressure at a height, *z*, above sea level, where *h* is the height of the top of the fluid column above sea level.

In all these rising magma source models, the conduit is initially empty. Magma then begins to fill the conduit at a constant speed *v*. When the conduit is full, the magma rise ceases instantaneously. The manner in which the flow starts and stops is not important; it is the size and shape of the seismic signals that result from the steady rise of the magma in the conduit that are of interest.

### 4.4.7 Rising magma with a pressure gradient

In this type of source, the pressure is changing by the same amount throughout a section of conduit, representing a line source. However, from one time step to another, the section of conduit over which the pressure change is occurring is increasing in length, so this as an expanding line source.

At the base of the conduit (*z=0*), the pressure rises by an amount $\rho gv$ in 1 second, as the weight of overlying magma increases. At some other height, *z*, in the conduit, the pressure remains unchanged until after a time *z/v*, which is the time required for magma to reach that level within the conduit. After this time, the

pressure will again begin to rise by amount $\rho gv$ every second. This can be expressed by:

$$\Delta P(z,t) = \rho g(vt - z)H(t - \frac{z}{v})B(z)_0^l \qquad \textbf{(4-67)}$$

using the notation developed in Appendix E. Notice the Heaviside function 'turns on' the pressure change at height *z* after time *z/v*. The Boxcar function ensures that this only occurs for points within the conduit (between *z=0* and *z=l*).

Using E-6, E-9, E-12, E-13 and E-14 this becomes:

$$\Delta P(k_z,\omega) = \frac{\rho g}{i\omega}\left\{\frac{v}{\omega \mathrm{K}} - \frac{e^{i\mathrm{K}l}}{k_z \mathrm{K}} - \frac{ve^{-i\omega\frac{l}{v}}}{\omega k_z}\right\} \qquad \textbf{(4-68)}$$

where $K = k_z - \frac{\omega}{v}$.

## *4.4.8 Rising overpressurised magma*

Very viscous magmas are often very highly overpressurised, and this can have explosive consequences. It would be useful therefore if volcano-seismologists could tell when overpressurised magma was nearing the surface, based on its seismic signature.

In this model the magma pressure is constant, i.e. there is no pressure gradient. Pressure is only changing at the point where magma is displacing the gases above it, but this point moves as the magma rises. Hence this is an example of a moving point source.

This is just another contribution to the overall pressure profile, since any rising magma must have a pressure gradient. However, in some cases the pressure gradient may have a small effect in comparison to the overpressure (particularly if the stations are close to the conduit[2]).

[2] The distance between a station and a moving point source changes more if that station is closer to the axis of the source. Stations which are close to the source are therefore very useful for distinguishing between moving point sources and other types of sources.

$\Delta P(z,t)$ is similar to 4-67, except here the magma pressure, $P_0$ is constant, which makes this a simpler case:

$$\Delta P(z,t) = P_0 H(t - \frac{z}{v}) B(z)_0^l \quad \textbf{(4-69)}$$

Using E-6, E-12 and E-13 this becomes:

$$\Delta P(k_z, \omega) = \frac{P_0}{\omega} \frac{1 - e^{iKl}}{K} \quad \textbf{(4-70)}$$

where $K$ has the same meaning as before.

### 4.4.9 Dynamic pressure of a rising magma

According to the Bernoulli equation, a moving fluid (in steady irrotational, incompressible, invisicid flow) has a dynamic pressure given by:

$$P_d = -\frac{1}{2} \rho v^2 \quad \textbf{(4-71)}$$

This is derived from conservation of energy along a streamline. However, assuming that this holds in this model, which may approximately be true, then the consequence is that points along the conduit wall suffer a pressure drop described by $P_d$ as they are 'overtaken' by the rising magma. For large $v$, this pressure drop may become a significant seismic source. However, one must bear in mind that magma rise velocities are very small (<1 m/s) except within a few hundreds of metres from the surface, where they may increase substantially, driven by the sharp reduction in friction that accompanies fragmentation. However, as magma rise speed increases, density drops. Mass flux, $Q$, is assumed to be equal throughout the conduit. Mass flux is given by:

$$Q = \rho \pi r_c^2 v \quad \textbf{(4-72)}$$

Combining this with 4-71 to eliminate $v$ yields:

$$P_d = -\frac{1}{2 \rho \pi^2 r_c^4} Q^2 \quad \textbf{(4-73)}$$

So the Bernoulli effect increases as the conduit radius reduces (because flow speed must increase to keep mass flux constant). Since the conduit radius is likely to increase with depth, the Bernoulli effect is only likely to be significant at shallow depths, if at all. However, there may be constrictions at some other points along the conduit, which act as seismic point sources, because the flow speeds up a great deal there. (Such constrictions are unlikely at such a steady volcano as Stromboli, but there may perhaps be such a constriction at the point where conduit and magma chamber meet).

Since this is a pressure drop which acts only at points as they are overtaken by the rising magma, this is again a moving point source. It can be modelled in exactly the same way as the overpressure source, simply substituting $P_d$ for $P_0$ (this is no longer true if changes in density or speed of the flow are allowed):

$$\Delta P(k_z,\omega) = \frac{P_d}{\omega}\frac{1-e^{iKl}}{K} \qquad \textbf{(4-74)}$$

### *4.4.10 Shear stress for a rising magma*

Changes in shear stress caused by rising magma can generate SV waves. Once the flow is initiated, magma rises at a constant speed *v* (in this model). Shear stress, $\tau$, only changes at points along the conduit wall as the magma rises above that level. This is another example of a moving point source. *Theisse* [1996] derived a relation for shear stress of a Newtonian fluid, $\tau$, in terms of radial distance, *r,* average flow velocity, *v*, and coefficient of viscosity, $\eta$:

$$\tau(r) = -\frac{4\eta v}{r} \qquad \textbf{(4-75)}$$

If the fluid is at rest, only pressure forces need to be considered. Shear stresses will dominate for viscous, fast rising magmas.

Shear stress is only non-zero between onset of flow, *t=0*, and cessation of flow, *t=l/v*, since it is proportional *v*. Hence using the notation of Appendix E, changes in shear stress are given by:

$$\Delta\tau(z,t) = \frac{4\eta v}{r_c} B(t)^{l/v}_{z/v} B(z)^{l}_{0} \qquad \textbf{(4-76)}$$

Using E-7 and E-12 this becomes:

$$\Delta\tau(k_z,\omega) = -\frac{\tau_0}{\omega}\left[\frac{e^{iKl}-1}{K} - e^{-i\omega l/v}\,\frac{e^{ik_z l}-1}{k_z}\right] \qquad \textbf{(4-77)}$$

This completes the derivation of sources related to magma rise.

### *4.4.11 Modelling a rising gas*

Above the level at which magma fragments, lava clots are entrained by rapidly rising and expanding gas. Rising gas can be modelled in just the same way as rising magma, i.e. as a combination of overpressure and dynamic pressure components (but without a pressure gradient, owing to its low density, and without a shear stress component because it is practically inviscid). This model does not consider the decompression of gas.

### *4.4.12 Modelling the rupture of a cap rock*

If the pressure in a sealed section of conduit continues to rise (perhaps due to advective overpressure) the seal, or cap rock, may eventually break. Pressure is then released in a series of steps, which decay exponentially in time, because the pressure drop is proportional to excess pressure divided by ambient pressure. Each step corresponds to the passage of a rarefaction wave which travels from the upper end of the conduit, to its base and back, expanding the fluid (and causing bubble growth) in its wake. Gas expires periodically through the rupture at first (choked flow) becoming more continuous as the excess pressure drops [*Kieffer and Sturtevant*, 1984]. Decompression would lead to a decreasing P wave speed in the fluid, so each step would take longer than the last. Therefore this type of signal would probably look like a sweep signal with exponentially decaying envelope and a frequency changing from high to low.

Since the pressure ahead of a rarefaction wave is always higher than that behind it, this mechanism can be modelled by a modification of the overpressure source (which also involved two different regions of pressure).

# 4.5 Tests of the model

## *4.5.1 P and S phases*

Two sets of vertical component synthetic seismograms (computed using the $k$-$\omega$ modelling technique) are compared to see if P and S phases could be identified. For both sets, a point source is activated at time 0 s with a step function source signature. P wave velocity is set at 1000 m/s and S wave velocity at 577 m/s, with stations at distances of 1 km, 4 km and 16 km.

Fig. 4.4a is the case where there is no impedance contrast between the fluid and the solid. In other words, there is no conduit, the point source is embedded directly into the rock. Inflexions corresponding to P wave onsets are clearly visible arriving at the stations at 1 s, 4 s and 16 s respectively, as expected from the combination of station distances and P wave speed. S waves are not observed because the source produces only P waves ($A_f$ non-zero, $C_f$=0).

Fig. 4.4b is the normal case where there is a significant impedance contrast between fluid and solid. In this case SV wave onsets are clearly visible at 1.7 s, 6.9 s, and 27.7 s, marked by a second inflexion. These SV waves are produced by mode conversions at the conduit wall. The P and S wave onsets are clearly

(a)

(b)

distinguishable, despite the fact that P and S waves overlap in time[3].

[3] P and S waves will overlap for all distances less than $T\left(1/\beta - 1/\alpha\right)^{-1}$ where *T* is the period of the signal, and $\alpha$ and $\beta$ are the P and S wave velocities respectively.

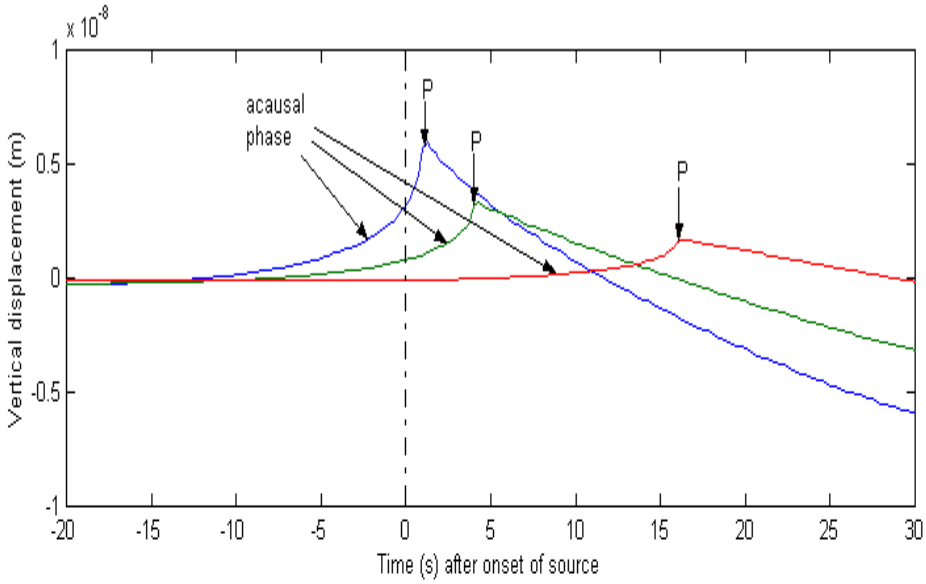
x 10^-8
Vertical displacement (m)
acausal
phase
P
P
P
Time (s) after onset of source

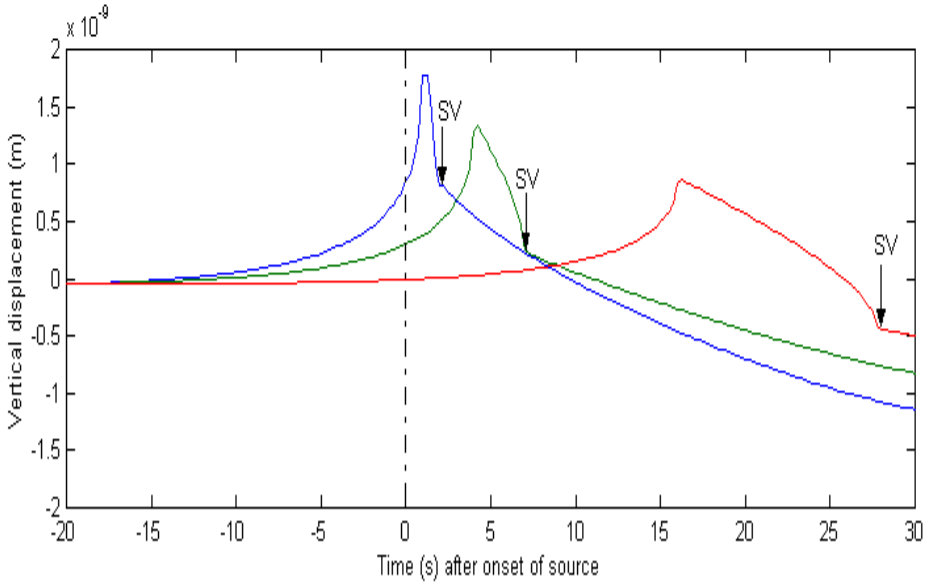
x 10^-9
Vertical displacement (m)
SV
SV
SV
Time (s) after onset of source

**Figure 4.4:** A point source (of P waves only) at *r*=0, *z*=0 in a narrow conduit is activated at *t*=0 s. The conduit is enclosed in a solid with a P wave speed of 1000 m/s and an S wave speed of 577 m/s. Synthetic seismograms are shown for stations at *r*=1000, *z*=0 (blue curve), *r*=4000, *z*=0 (green curve) and *r*=16000, *z*=0 (red curve), for two different models: (a) There is no impedance contrast at the conduit wall, so no conversion to SV waves occurs. The P wave arrivals, marked by an inflexion, are observed at the expected times – 1 s, 4 s and 16 s respectively. Prior to the P wave there is acausal energy which must be an artefact of the modelling scheme. (b) With a large impedance contrast at the conduit wall, partial conversion of P waves to SV waves does occur. This is confirmed by a decrease in the amplitude of the P phase, and a second inflexion marking the arrival of the SV phase at 1.7 s, 6.9 s and 27.7 s respectively.

There is a signal (marked on Fig. 4.4a as the 'acausal phase') prior to the P wave arrivals. This is physically meaningless because in a homogeneous medium, nothing travels faster than a direct P wave, so it must be an artefact of the modelling method, perhaps because a limited range of frequencies (0.015 – 2 Hz) were used to represent an impulsive source. Any similarity of these waveforms to the VLP signals at Stromboli is purely coincidental. Some further investigation of this acausal phase is warranted.

### *4.5.2 Relation between displacement and source volume*

The simple modelling performed in Chapter 3 showed that displacement in the near field is proportional to source volume for both point sources and line sources. These conclusions are supported by the more accurate *k*-ω modelling. Fig. 4.5 shows the maximum displacements produced by point sources of various volumes; both graphs are of the form *y=mx*, indicating displacement and source volume are proportional. An expression for the displacement from a point source in terms of pressure change and initial source volume is:

$$\left|\mathbf{u}\right| = k\Delta P V_0 \qquad \textbf{(4-78)}$$

where *k* is some constant. This is derived by combining 4-62 and 4-63.

Fig. 4.6 shows the maximum displacements produced by line sources of various cross-sectional areas; again these are exactly proportional. Hence, 4-78 also holds true for a line source.

For a rising magma source which has only a shearing component, we again expect displacement to be proportional to source volume and shear stress, $\tau$, (which takes the place of pressure), leading to an expression of the form:

$$|\mathbf{u}| = k\tau r^2 \qquad \textbf{(4-79)}$$

Figure 4.5

Figure 4.6

Using 4-74 this becomes:

$$|\mathbf{u}| = k\eta v r \qquad \textbf{(4-80)}$$

However, the results of $k$-$\omega$ modelling show that displacement and conduit radius are independent [Fig. 4.7] for a source involving only shear stress.

### *4.5.3 Decay laws*

To check whether the $k$-$\omega$ modelling method approximates near field terms adequately the decay laws from a point source [Fig. 4.8] and a line source [Fig. 4.9] were modelled. This was done for seismometers in the range of 0-5 km since most volcano-seismic stations are deployed within 5 km of the summit.

For a point source, Fig. 4.8 shows that the near field term dominates for $r<0.6\lambda$, where $\lambda$ is the maximum wavelength present in the source. In the near field the decay law approaches $1/r^2$. In Chapter 3 it was shown that the near field term dominated for $r<\lambda$. The discrepancy is possibly explained because the modelling here assumed a range of wavelengths, whereas the simple modelling assumed a monochromatic source.

The decay laws for a finite line source are more complicated [Fig. 4.9], because two different effects must be considered. First the finite line source begins to behave more like a point source for $r>L/2$, which corresponds to the distance at which the source subtends an angle of 80° at the station. Secondly the far field term begins to dominate for $r > 0.5\lambda$. In Chapter 3 it was concluded that the near field term dominated for $r<\lambda$; again the discrepancy can be explained because a range of wavelengths is used in this chapter, as opposed to the single frequency source used in Fig. 3.5. Decay laws for finite line sources always behave like $1/r$ for very near and very far sources, but for intermediate distances any behaviour is possible from $1/r^2$ to almost no decay at all.

The short-period wavefield at Stromboli corresponds to wavelengths of ~ 350 – 1700 m whereas the VLP wavefield wavelengths of 5 - 50 km. Figs. 4.8 and 4.9 suggest therefore that VLP phases can be observed to a much greater range. VLP signals from Aso volcano have been recorded up to distance of a few hundred kilometres [*Kawakatsu et al.,* 1994].

Figure 4.7

Figure 4.8

FIGURE 4.9

Decay law for line source.

### 4.5.4 Depression of the volcanic summit in response to rising magma

What happens at a station close to the conduit when rising magma 'overtakes' it? A conduit of length $l$=1000 m with stations at $r$=10, 100 and 1000 m, $z$=500 m, and a magma rise velocity of 1 m/s was used [Fig. 4.10]. If the $k_z$-$\omega$ modelling method works, some dramatic effects should be seen around 500 s (the amount of time required for magma to reach the level of the station in this example). Fig. 4.11a shows that the station moves radially outwards very rapidly as the magma reaches a level of ~500 m. Fig. 4.11b is more interesting - it shows that the station moves vertically *downwards* as magma rises up the conduit; this occurs because the summit of the volcano loses support as material below is pushed radially outwards by the pressurised rising magma. This is important because it predicts magma rising at depth leads to a depression of the volcanic summit. Note, however, that $\Delta P$ acts only to the sides (conduit walls). The particle motion is shown in Fig. 4.12.

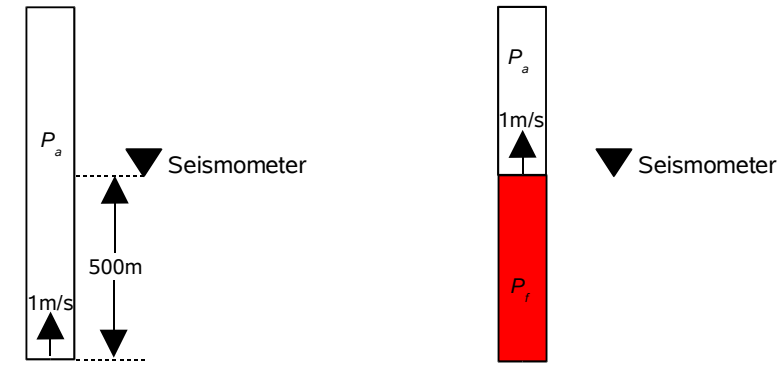


(a) t=0 s (b) t=500 s

**Figure 4.10:** (a) The conduit is empty at time $t$=0 s and at atmospheric pressure ($P_a$). Rising magma with pressure ($P_f$) starts to fill the conduit at a speed of 1 m/s, causing variations in the displacement of the seismometer. The strongest effects are felt around 500 s, when the moving source makes its closest approach to the conduit.

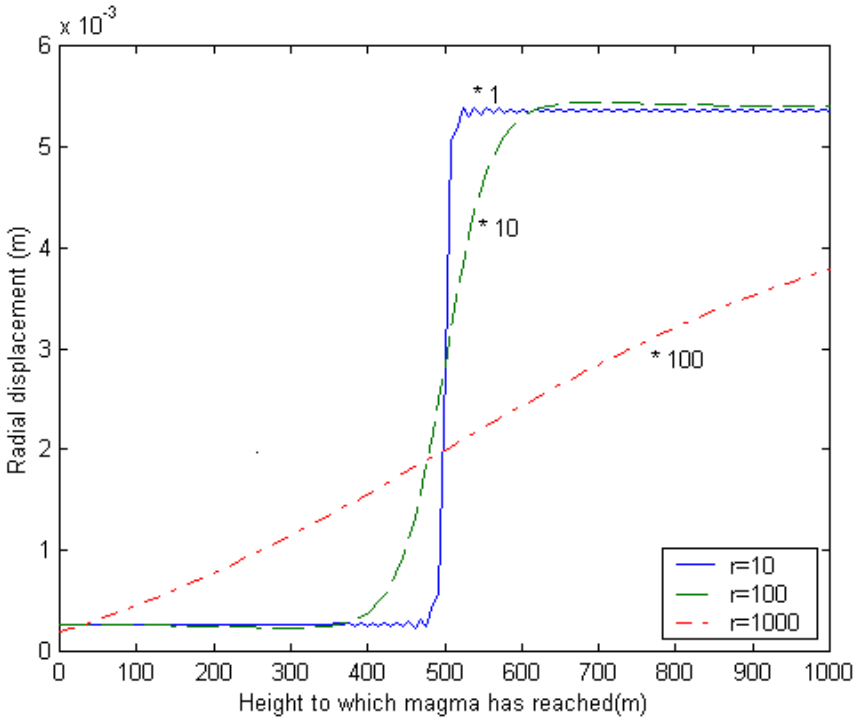
x 10^-3
Radial displacement (m)
Height to which magma has reached(m)
* 1
* 10
* 100
r=10
r=100
r=1000
0
1
2
3
4
5
6
0
100
200
300
400
500
600
700
800
900
1000

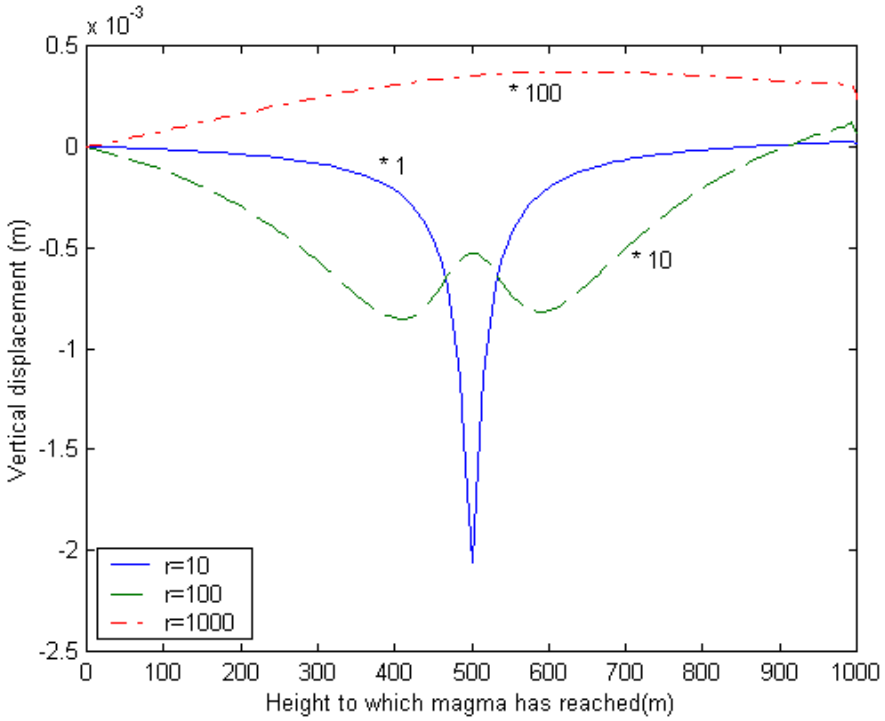


(b)

**Figure 4.11:** Overpressurised magma (a moving point source) rises up a conduit of length 1000 m at 1 m/s. Seismograms are shown for stations half-way up the conduit, at radial distances, *r*, of 10, 100 and 1000 m respectively (magnifications are also shown). (a) Radial displacements show that stations nearer the conduit have a more implusive reaction, since they experience the source as a more local effect. (b) Vertical displacements show behaviour as radial distance increases. For stations near the conduit, the initial motion is downwards, even though the source is a pressure increase. This motion becomes more exaggerated as the source approaches. After nearest approach, the vertical motion reverses. For stations far from the conduit, the motion is upwards prior to nearest approach, and then downwards. For stations at intermediate distances the vertical motion is more complicated.

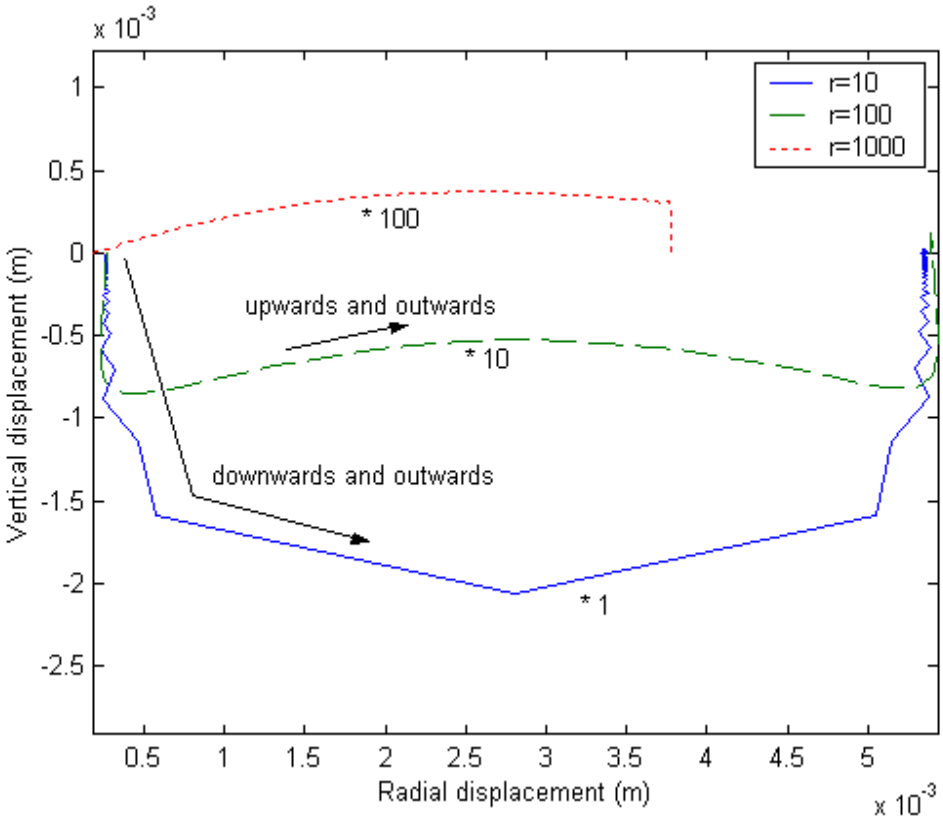


**Figure 4.12:** Particle motion at different radial distances from the conduit. This demonstrates that for stations very close to the conduit (~100 m), subsidence may be observed in response to rising magma, but this could easily be interpreted as deflation of the volcano. At greater distances particle motions reveal that the volcano is in fact inflating. See figure 4.11 for more details.

However, such an observation could easily be interpreted as a depressurisation of a spherical magma body (using the Mogi model), thus leading to an entirely wrong assessment of volcanic hazard.

When the rising magma gets close to the station, the station is pushed radially outwards and upwards, recovering some of its lost height. When the magma level finally overtakes the station, the station is pushed radially outwards and downwards. Finally, as the rising magma moves material above the station radially outward, the weight of overlying material is reduced, and the station moves upwards again, recovering nearly all of its lost height (not all, because the end result is that the pressure along the entire conduit has increased).

### 4.5.5 Superposition of sources

The effects of pressure and shear stress are independent [Fig. 4.13]. This is useful as it means that for a particular model, the effects of a certain pressure, and the effects of a certain shear stress can be investigated independently. Furthermore this allows the seismograms for any linear combination of pressure and shear stress to be computed simply by linear combination of the seismograms. In the case of rising magma it is also valid to form linear combinations of different pressure terms such as overpressure, pressure gradient and dynamic pressure. This important result suggests that the best way to study rising magma is to study the effects of each pressure term and the shear stress term independently.

### 4.5.6 Source reconstruction

The source representations that are fed into the method (e.g. equations 4-64, 4-67 and 4-69) can be reconstructed using the discrete wavenumber method, which is the same method used to calculate synthetic seismograms. If the reconstructed source matches the source representation that was used, it means that the Fourier transforms used in Appendix E are correct, and that the discrete wavenumber method works. This increases our confidence in the computed synthetic seismograms. For example, consider the representation for an overpressurised rising magma source:

$$\Delta P(z,t) = P_0 H(t - \frac{z}{v}) B(z)_0^l \qquad \textbf{(4-69)}$$

Which after a double Fourier transform to the $k_z$-$\omega$ domain becomes:

$$\Delta P(k_z, \omega) = \frac{P_0}{\omega} \frac{1 - e^{iKl}}{K} \qquad \textbf{(4-70)}$$

Figure 4.13

This is the formula which is coded. Now in the same way that seismograms are calculated, the pressure time series can be calculated from the modelling technique. The pressure time series (at several depths) obtained as an output from the modelling technique should be consistent with the source that was being modelled, in this case an overpressurised rising magma.

The method for calculating the integral:

$$\mathbf{u}_s(\mathrm{z},\mathrm{t}) = \frac{1}{2\pi}\int_{-\infty}^{\infty}\left(\frac{1}{2\pi}\int_{-\infty}^{\infty}\mathbf{u}_s(k_z,\omega)e^{-ik_z z}\,dk_z\right)e^{i\omega t}\,d\omega \qquad \textbf{(4-46)}$$

is to approximate it by:

$$\mathbf{u}_s(\mathrm{z},\mathrm{t_c}) = \frac{e^{\omega_i t_c}}{2\pi}\delta\omega_m\sum_{m=-M}^{M}\left(\frac{\delta k_z}{2\pi}\sum_{n=-N}^{N}\mathbf{u}_s(k_z,\omega)e^{-ik_n z}\right)e^{i\omega_m t_c} \qquad \textbf{(4-57)}$$

where the inner summation is the discrete wavenumber method. The pressure time series can be reconstructed in the same way:

$$P(\mathrm{z},\mathrm{t_c}) = \frac{e^{\omega_i t_c}}{2\pi}\delta\omega_m\sum_{m=-M}^{M}\left(\frac{\delta k_z}{2\pi}\sum_{n=-N}^{N}P(k_z,\omega)e^{-ik_n z}\right)e^{i\omega_m t_c} \qquad \textbf{(4-81)}$$

This was included in the code. The model used was a 1000 m long conduit, with magma rising at 1 m/s, with an overpressure of 1 MPa. The pressure time series at heights of 500 m and 700 m above the base of the conduit were calculated [Fig. 4.14]. The results show that for z=500 m, the pressure increases by 1 MPa after 500 s. This is expected because at time the magma would have risen to 500 m above the base of the conduit. The same pressure rise occurs after 700 s at z=700 m, demonstrating that the source representation for an overpressurised rising magma, and the method for calculating seismograms are both sound. Further checking revealed that the source representations for a line source, a rising magma with a pressure gradient and with shear forces also give the expected results.

FIGURE 4.14

Source step functions.

## 4.6 Conclusions

In this Chapter, a method for calculating synthetic seismograms/deformation has been derived for three types of sources within a cylindrical conduit:

1) point sources,
2) pressurisation of a conduit section (line source),
3) magma rise, which has four components which can be superposed:
    a) pressure gradient (expanding line source),
    b) overpressure (moving point source),
    c) dynamic pressure (moving point source),
    d) shear stress (moving point source).

In addition, a rising bubble has been synthesised by staggering in time several point sources acting at different positions, and models for a rupture source and a rising gas (modifications to the rising magma model) were discussed. Testing of modelling method revealed that:

(i) P and S waves are correctly delayed.

(ii) The method used for feeding different sources into the modelling technique works, because the pressure source function (and the shear stress source function) recovered was as expected in all cases.

(iii) Decay laws show that near field effects are included in models.

(iv) Increasing the impedance contrast between fluid and solid leads to reduced amplitude of seismic waves in the solid *i.e.* coupling is reduced as expected.

(v) Solutions can be linearly combined as the effects of the different source components are independent (because stress is assumed proportional to strain),

(vi) Dramatic effects are seen at stations close to the conduit as magma rises past them. Surprisingly, these stations move downwards before magma reaches

them, which is explained by the rock below them being pushed radially outwards.

In Chapter 5 the techniques derived in this chapter will be applied to Stromboli.